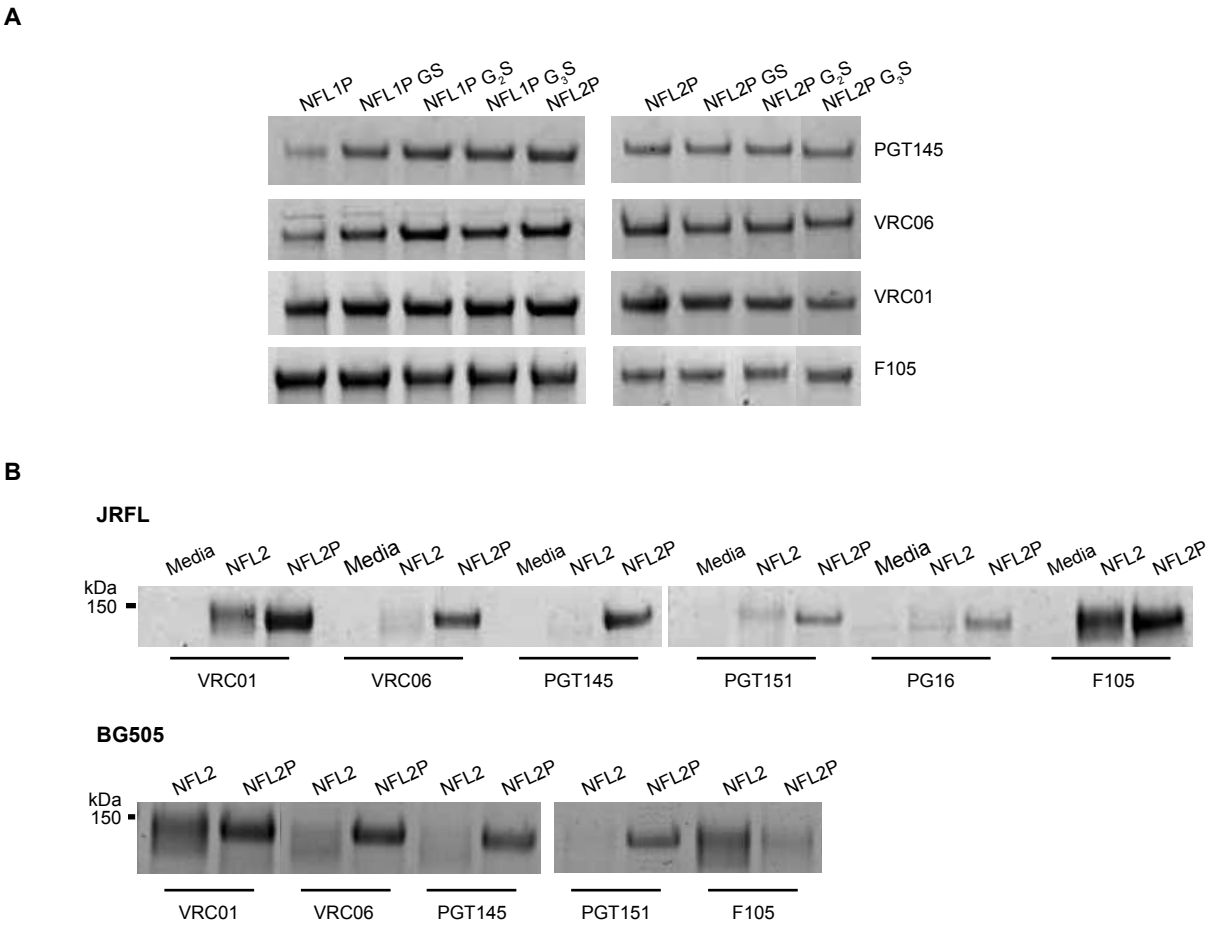

Figure S1. Optimization of NFL linker length and expression, related to Figure 1.
(A) The NFL linker length was further optimized with a stepwise addition of one residue between NFL1P and NFL3P. Relative well-ordered trimer expression was assessed by IP with the trimer preferring bNAbs PGT145 and VRC06 compared to VRC01 and non-NAb F105. (B) Necessity of I559P mutation in the NFL context was evaluated by IP using a select panel of mAbs. JRFL (top) and BG505 (bottom) gp140 NFL2 were expressed without or with (NFL2P) the I559P change. (C) SDS-PAGE of lectin-purified JRFL and BG505 gp140 NFL2P is shown.

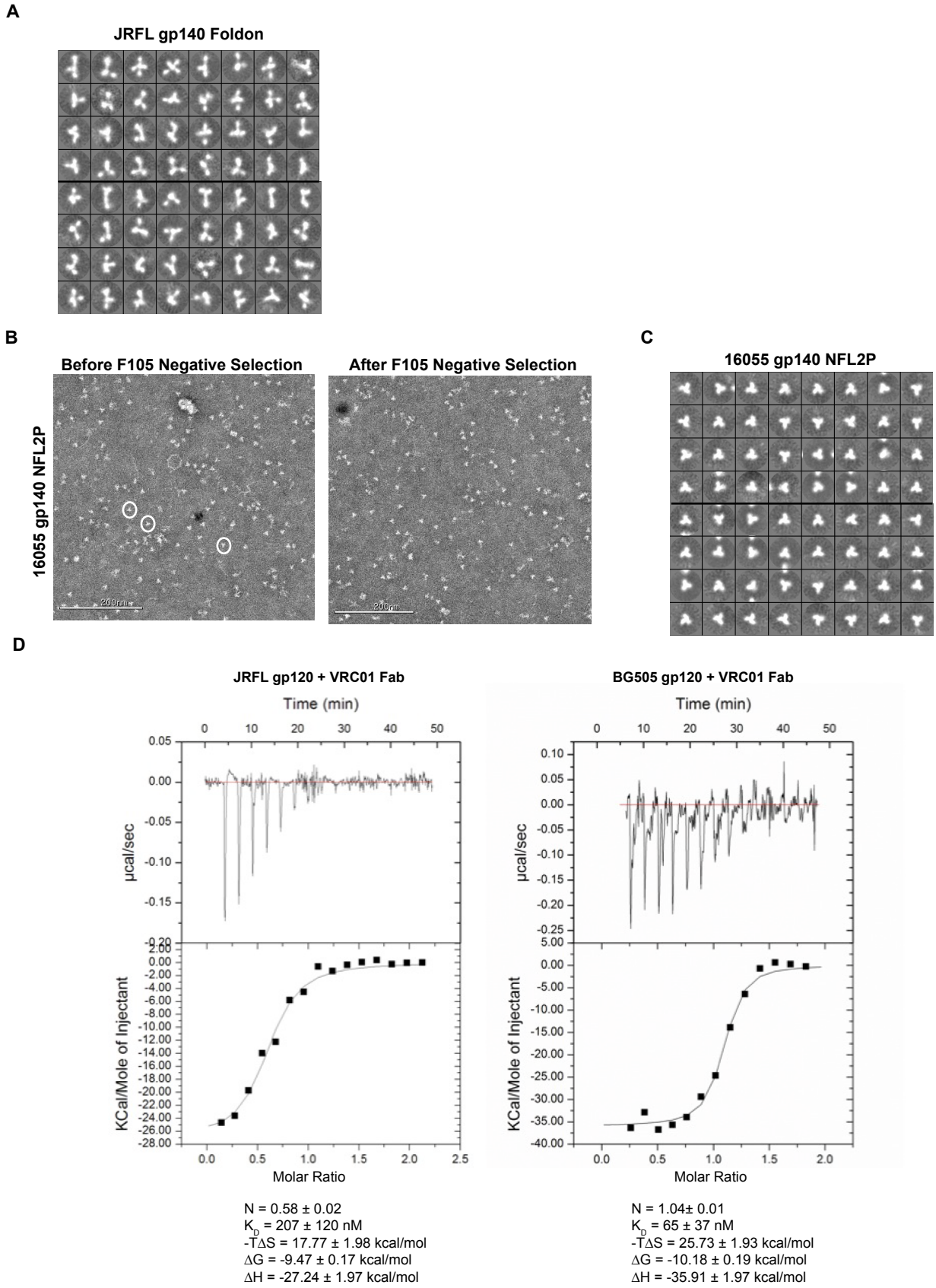

Figure S2. Negative Stain EM of JRFL gp140-foldon and 16055 gp140 NFL2P along with thermodynamic analysis of JRFL and BG505 gp120 by ITC, related to Figure 3. (A) EM 2D class averages of unliganded JRFL gp140-foldon. (B) Negative stain EM micrographs of 16055 gp140 NFL2P before and after F105 negative selection. Within the SEC isolated trimer fraction, well-ordered trimeric proteins (circled) along with disordered oligomers are detected before negative selection (left), while the negatively selected sample contains well-ordered trimeric proteins (right). Scale bars, 200 nm. (C) EM 2D class averages of unliganded 16055 gp140 NFL2P. (D) The raw data (top) and binding isotherms (bottom) from ITC measuring the binding of JRFL (left) and BG505 (right) gp120 to VRC01 Fab are shown.

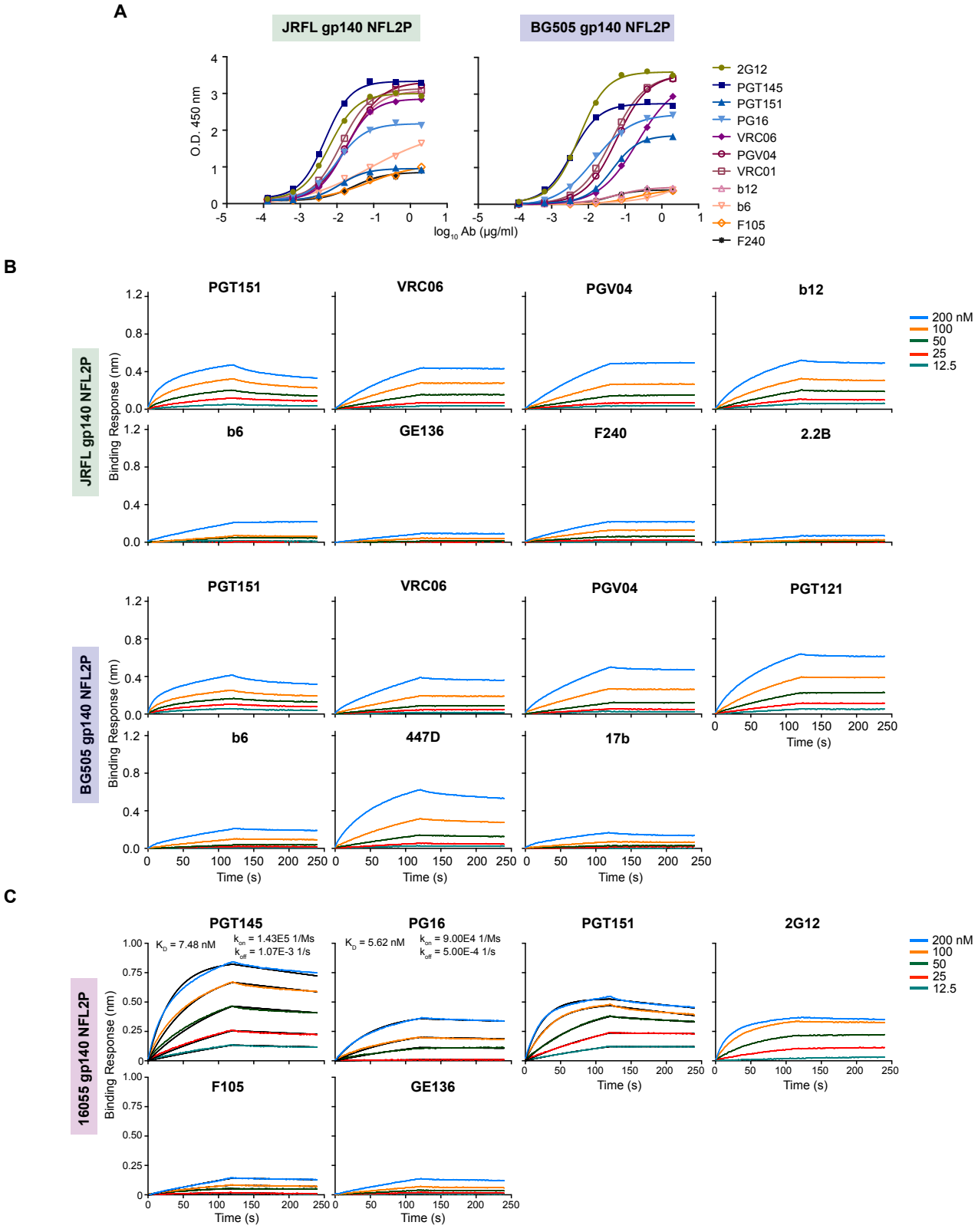

Figure S3. Antigenicity of NFL2P trimers by ELISA and BLI, related to Figure 4.
(A) Binding of selected mAbs to JRFL (left) and BG505 (right) gp140 NFL2P trimers by ELISA with the trimers captured by an anti-His mAb coated on the plate to maintain proper orientation. Trimer specific bNAbs (PGT145, PGT151, PG16, and VRC06), bNAbs (2G12, PGV04, VRC01, and b12) and non-NAbs (b6, F105, and F240) were assessed. Binding profiles of additional mAbs to (B) JRFL and BG505 gp140 NFL2P and (C) 16055 gp140 NFL2P by BLI are shown. Anti-human Fc sensors were used to capture the mAbs and the NFL2P proteins were used as an analyte at various concentrations (200-12.5 nM). The black curves for PG145 and PG16 in (A) and PGDM1400 and VRC26 in (B) depict theoretical Langmuir fits generated by 1:1 binding kinetics. Trimer-specific bNAbs (PGT145, PG16, PGT151, VRC06), CD4bs-directed bNAbs (PGV04, b12), glycan-specific bNAbs (2G12, PGT121), non-broadly neutralizing mAbs (b6, GE136, F105, F240, 2.2B, 447D, 17b) are shown.

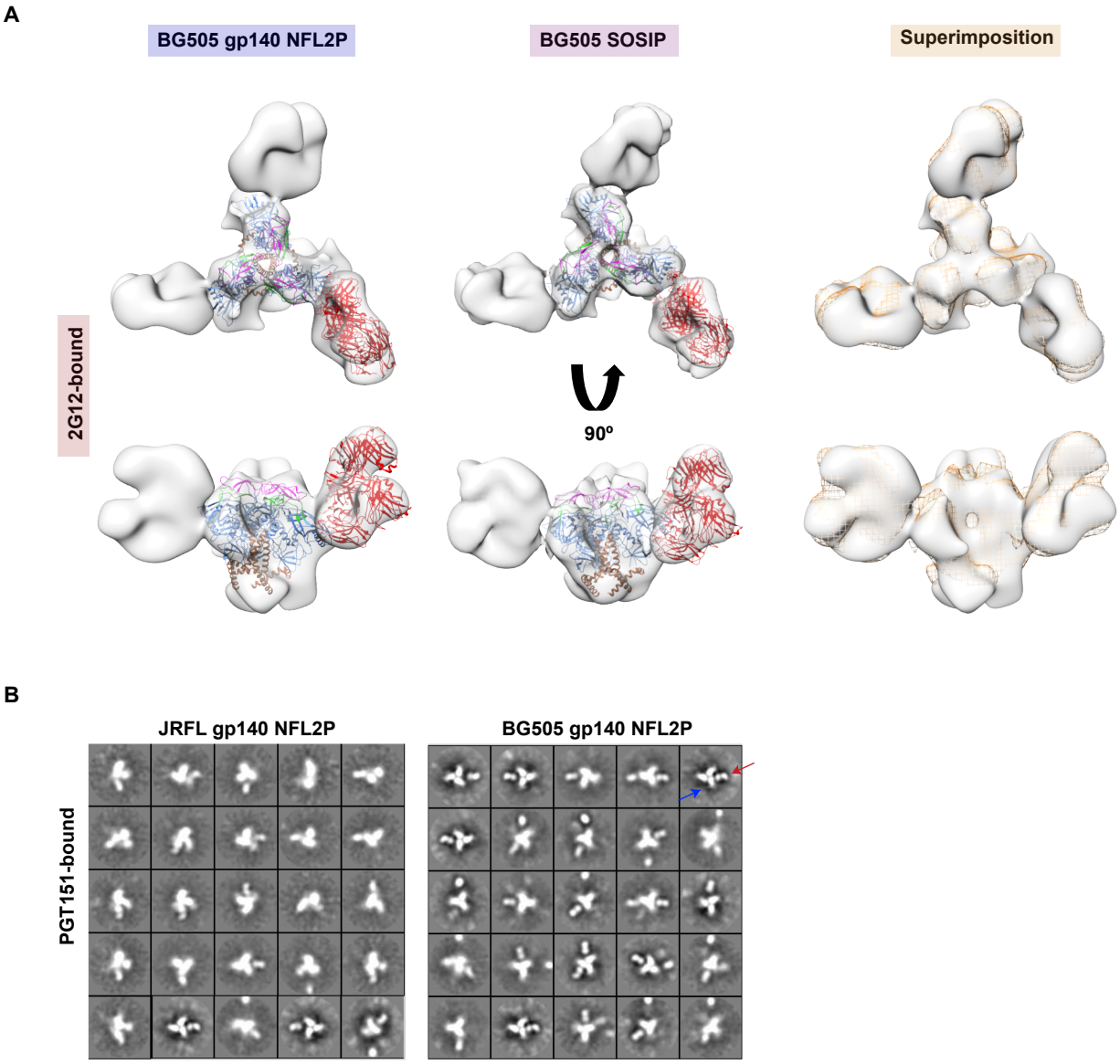

Figure S4. EM 3D reconstructions of 2G12-liganded BG505 gp140 NFL2P and BG505 SOSIP.664 trimers and 2D class averages of PGT151-bound to the uncleaved trimers, related to Figure 6 and Table S2.
(A) Top and side views of 3D reconstruction EM densities of 2G12-bound BG505 gp140 NFL2P and BG505 SOSIP.664 trimers (gray) with the BG505 SOSIP.664 structure (PDB 3J5M; gp120 in blue, V1V2 in magenta, V3 in green and gp41 in brown) and 2G12 crystal structure (PDB 1OP5; 2G12 in red) fitted within. To the right, top and side views of the 2G12 bound BG505 SOSIP.664 EM density (orange) superimposed onto the BG505 gp140 NFL2P density (gray). (B) EM 2D class averages of PGT151-bound JRFL and BG505 NFL gp140 NFL2P trimers (left and right, respectively). Red arrows indicate the density corresponding to a PGT151 Fab and the blue arrows indicate the density corresponding to Env.

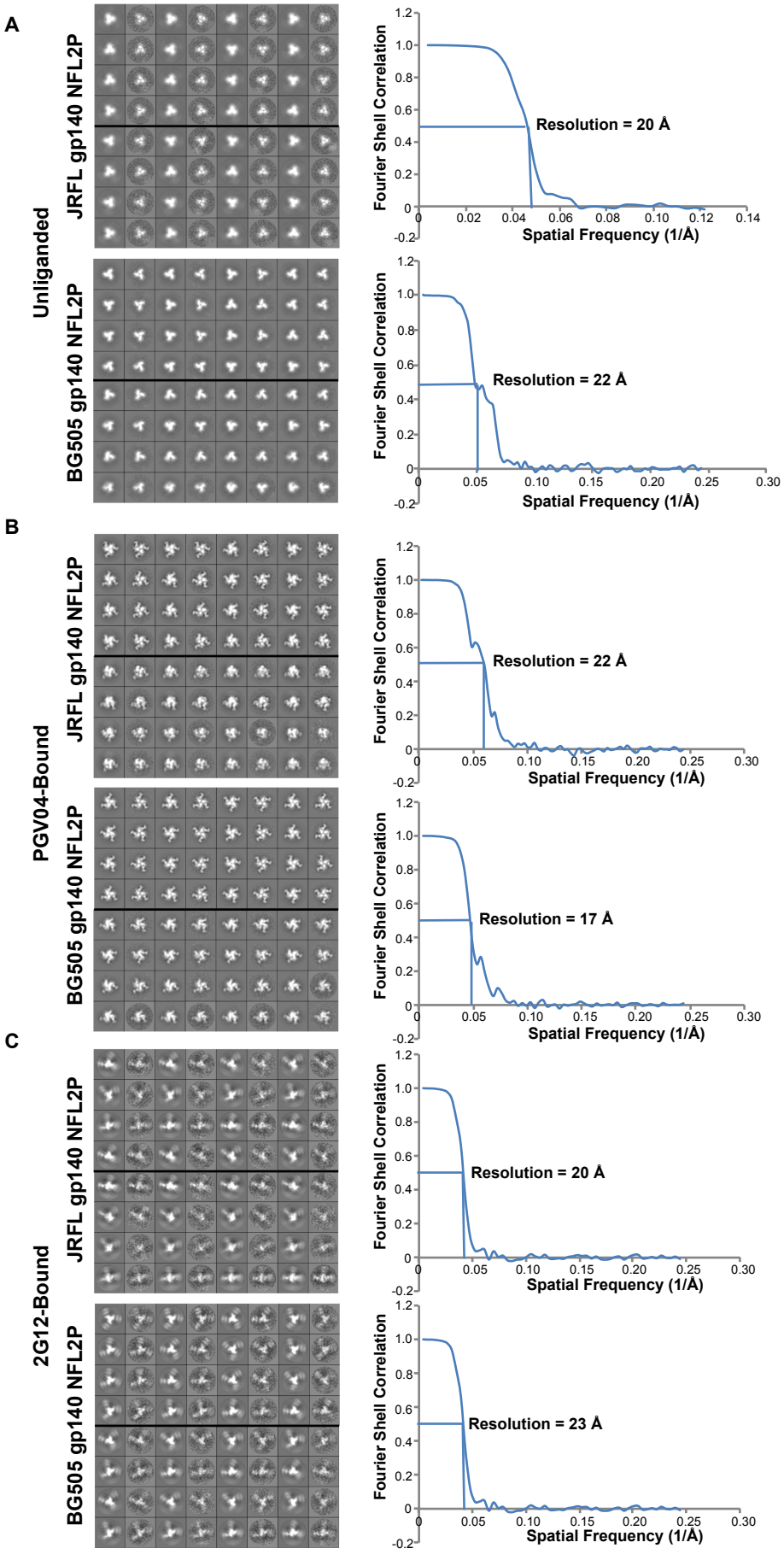

Figure S5. Projection matching and Fourier Shell Correlation graphs, related to Figure 6 and Table S2.
(A) Unliganded JRFL (top) and BG505 (bottom) gp140 NFL2P trimers. (B) PGV04-bound JRFL (top) and BG505 (bottom) gp140 NFL2P trimers. (C) 2G12-bound JRFL (top) and BG505 (bottom) gp140 NFL2P trimers.

Table S1. Binding kinetics of trimer-specific bNAbs to JRFL and BG505 gp140 NFL2P, SOSIP, and foldon trimers as observed by BLI, related to Figures 4 and S3.

bNAb	Env	K_D (nM)	k_{on} (1/Ms)	k_{off} (1/s)	R^2
PGT145	JRFL gp140 NFL2P	1.67	1.16E5	1.93E-4	0.99
	JRFL SOSIP	0.55	1.14E5	6.27E-5	0.99
	BG505 gp140 NFL2P	8.51	3.13E5	2.66E-3	0.99
	BG505 SOSIP	4.37	2.31E5	1.01E-3	0.99
	JRFL gp140 Foldon	NB	NB	NB	---
PG16	JRFL gp140 NFL2P	23.26	1.88E5	4.38E-3	0.99
	JRFL SOSIP	23.01	1.21E5	2.79E-3	0.99
	BG505 gp140 NFL2P	21.29	1.64E5	3.49E-3	0.99
	BG505 SOSIP	14.83	1.45E5	2.08E-3	0.99
	JRFL gp140 Foldon	NB	NB	NB	---
PGDM1400	JRFL gp140 NFL2P	43.50	4.60E4	2.00E-3	0.99
	JRFL SOSIP	58.90	2.65E4	2.70E-3	0.99
	BG505 gp140 NFL2P	10.60	1.71E5	1.82E-4	0.99
	BG505 SOSIP	4.40	1.60E5	7.10E-4	0.99
	JRFL gp140 Foldon	NB	NB	NB	---
VRC26	JRFL gp140 NFL2P	NB	NB	NB	---
	JRFL SOSIP	NB	NB	NB	---
	BG505 gp140 NFL2P	21.29	1.64E5	3.49E-3	0.99
	BG505 SOSIP	14.83	1.45E5	2.08E-3	0.99
	JRFL gp140 Foldon	NB	NB	NB	---

Table S2. Binding stoichiometries of bNAbs to JRFL and BG505 gp140 NFL2P trimers as observed by negative stain EM and particles used for 3D EM reconstruction, related to Figures 5-6 and S4-5.

Env	Fab	Unliganded	1 Fab Bound	2 Fabs Bound	3 Fabs Bound	# Particles
JRFL gp140 NFL2P	Unliganded	-	-	-	-	29376
	PGV04	2%	18%	35%	45%	273335
	2G12	10%	15%	20%	55%	9311
	PGT151	91%	9%	0%	0%	-
BG505 gp140 NFL2P	Unliganded	-	-	-	-	34047
	PGV04	3%	10%	13%	74%	26948
	2G12	7%	18%	25%	50%	10053
	PGT151	36%	44%	19%	1%	-

Supplemental Experimental Procedures

Electron microscopy

A 3 μL aliquot containing ~0.05 mg/ml of the Fab and trimer complex was applied for 15 s onto a carbon coated 400 Cu mesh grid that had been glow discharged at 20 mA for 30 s, then negatively stained with 2% uranyl formate for 30 s. Data were collected using a FEI Tecnai Spirit electron microscope operating at 120 keV, with an electron dose of ~30 $e^-/Å^2$ and a magnification of 52,000x that resulted in a pixel size of 2.05 Å at the specimen plane. Images were acquired with a Tietz 4k X 4k TemCam-F416 CMOS camera using a nominal defocus of 1000 nm and the Leginon package (Suloway et al., 2005) at 10° tilt increments, up to 50°. The tilts provided additional particle orientations to improve the image reconstructions.

Data processing, image reconstruction, and model fitting

Particles were picked automatically using DoG Picker and put into a particle stack using the Appion software package (Lander et al., 2009; Voss et al., 2009). Initial, reference-free, 2D class averages were calculated using particles binned by two via Xmipp Clustering 2D Alignment (Sorzano et al., 2010) and sorted into classes. Particles corresponding to complexes were selected into a substack and binned by two before another round of reference-free alignment was carried out using the Xmipp Clustering and 2D alignment and IMAGIC programs (van Heel et al., 1996). Fabs were clearly visualized in the 2D class averages if they are bound to the trimer, allowing the percentage of bound trimers relative to unbound trimers to be tabulated. *Ab initio* common lines models were calculated from reference-free 2D class averages in EMAN2 (Tang et al., 2007) without imposing symmetry. All *ab initio* common lines models were the same. One of those models was then refined against raw particles for an additional 89

cycles. EMAN was used for the 3D reconstructions. Resolutions of the final models were determined using a Fourier Shell Correlation (FSC) cut-off of 0.5 (Figure S5), and the number of particles used for each 3D reconstruction is summarized in Table S1.

Supplemental References

Lander, G.C., Stagg, S.M., Voss, N.R., Cheng, A., Fellmann, D., Pulokas, J., Yoshioka, C., Irving, C., Mulder, A., Lau, P.W.*, et al.* (2009). Appion: an integrated, database-driven pipeline to facilitate EM image processing. Journal of structural biology *166*, 95-102.

Pettersen, E.F., Goddard, T.D., Huang, C.C., Couch, G.S., Greenblatt, D.M., Meng, E.C., and Ferrin, T.E. (2004). UCSF Chimera--a visualization system for exploratory research and analysis. Journal of computational chemistry *25*, 1605-1612.

Sorzano, C.O., Bilbao-Castro, J.R., Shkolnisky, Y., Alcorlo, M., Melero, R., Caffarena-Fernandez, G., Li, M., Xu, G., Marabini, R., and Carazo, J.M. (2010). A clustering approach to multireference alignment of single-particle projections in electron microscopy. Journal of structural biology *171*, 197-206.

Suloway, C., Pulokas, J., Fellmann, D., Cheng, A., Guerra, F., Quispe, J., Stagg, S., Potter, C.S., and Carragher, B. (2005). Automated molecular microscopy: the new Leginon system. Journal of structural biology *151*, 41-60.

Tang, G., Peng, L., Baldwin, P.R., Mann, D.S., Jiang, W., Rees, I., and Ludtke, S.J. (2007). EMAN2: an extensible image processing suite for electron microscopy. Journal of structural biology *157*, 38-46.

van Heel, M., Harauz, G., Orlova, E.V., Schmidt, R., and Schatz, M. (1996). A new generation of the IMAGIC image processing system. Journal of structural biology *116*, 17-24.

Voss, N.R., Yoshioka, C.K., Radermacher, M., Potter, C.S., and Carragher, B. (2009). DoG Picker and TiltPicker: software tools to facilitate particle selection in single particle electron microscopy. Journal of structural biology *166*, 205-213.